

Quasi-collective motion of nanoscale metal strings in metal surfaces

M. LABAYEN¹, C. RAMIREZ², W. SCHATTKE² AND O. M. MAGNUSSEN^{1*}

¹Institut für Experimentelle und Angewandte Physik, Universität Kiel, 24098 Kiel, Germany

²Institut für Theoretische Physik und Astrophysik, Universität Kiel, 24098 Kiel, Germany

*email: magnussen@physik.uni-kiel.de

Published online: 2 November 2003; doi:10.1038/nmat1011

Mass transport processes on metal surfaces play a key role in epitaxial growth and coarsening processes. They are usually described in terms of independent, statistical diffusion and attachment/detachment of individual metal adatoms or vacancies^{1,2}. Here we present high-speed scanning tunnelling microscopy (video-STM) observations of the dynamic behaviour of five-atom-wide, hexagonally ordered strings of Au atoms embedded in the square lattice of the Au(100)-(1×1) surface that reveal quasi-collective lateral motion of these strings perpendicular to as well as along the string direction. The perpendicular motion can be ascribed to small atomic displacements in the strings induced by propagating kinks, which also provides a mechanism for the exchange of Au atoms between the two string ends, required for motion in string direction. In addition, quasi-one-dimensional transport of Au adatoms along the string boundaries may contribute to the latter phenomenon according to density functional calculations.

The reconstructed Au(100) surface exhibits a hexagonally ordered topmost layer with a 25% higher packing density than the underlying square Au lattice, resulting in a uniaxial, vertical modulation of the Au surface layer^{3–5}. It is a prototypical example of a striped adlayer phase and structurally identical to phases found on other reconstructed f.c.c.(100) surfaces³ as well as in many heteroepitaxial metal⁶ and non-metallic adlayers⁷ on square substrates. In this work, the Au surface dynamics was studied in an electrochemical system, where a reversible phase transition between the ‘hex’ reconstructed and the unreconstructed (1×1) phase can be induced by the electrode potential^{8–13}. The formation of this potential-induced reconstruction negative of a critical potential proceeds through nucleation and growth of small, strongly anisotropic ‘hex’ domains parallel to the {110} directions and exhibiting one or several ≈ 14.5 -Å-wide strings^{11–13}. Each ‘hex’ string consists of five hexagonally ordered rows of Au surface atoms (Fig. 1a,b), which are displaced from the fourfold-hollow sites in the underlying bulk (100) lattice, corresponding to a uniaxial, vertical modulation of the Au surface layer (indicated by the different shading in the models). Two types of strings exist with the Au atoms at the ‘hex’-(1×1) boundary (dashed lines) being out-of-phase (Fig. 1a) or in-phase (Fig. 1b), resulting in a single (Fig. 1a) or double (Fig. 1b and Fig. 1c,d) ridge of elevated atoms in atomic-resolution STM images. As will be shown below, these elementary units of the Au(100) reconstruction are highly mobile objects. Detailed data on the dynamic behaviour of the ‘hex’ strings

could therefore not be obtained in studies by conventional STM^{11–13}, where 30–200 s are required for the acquisition of a single STM image.

Using a novel *in situ* high-speed STM developed in our group^{14,15}, however, the ‘hex’ string dynamics is readily accessible. After a potential step from +0.45 V (versus saturated calomel electrode), where the Au surface is unreconstructed, to –0.1 V, the growth of isolated ‘hex’ strings along the two main directions of the square (100) lattice is observed (a full video is provided as Supplementary Information). High-resolution *in situ* video-STM images of these isolated strings reveal frequent lateral displacements in the direction perpendicular to the string (Fig. 1c,d), as already noticed in the previous studies^{12,13}. These displacements manifest in the form of sudden shifts of the ‘hex’ strings by one or several Au lattice distances (marked by arrows) during the recording of the images. As the surrounding (1×1) lattice or other ‘hex’ strings (see for example, Fig. 1d) are not shifted at the position of the jump, a change in the ‘hex’ string position due to experimental artifacts, such as lateral jumps of the STM tip, can be excluded. Furthermore, the presence of the tip does not significantly enhance the string mobility under the tunnelling conditions used in this work, as verified by systematic studies. In most events displacements of one (Fig. 1c, white arrow) or two (Fig. 1c,d black arrow) surface lattice spacings a_{Au} are observed, which usually occur within one or two scan lines, that is, within ≤ 300 μ s for images recorded at 15 frames per second. The jumps result in a random motion of ‘hex’ strings easily visible in video-STM sequences. This is illustrated in Figs 2a and 3a for ‘hex’ strings running approximately perpendicular and approximately parallel to the slow scan direction (that is, in the x and y directions, respectively). For ‘hex’ strings oriented roughly parallel to the y direction (Figs 1c and 3a) the lateral jumps result in a ‘wiggly’ appearance, with jumps occurring on average every 25 ms (pinning by neighbouring strings or Au steps, however, can strongly reduce the string mobility). In contrast, strings in the x direction, where the entire row is recorded within a few scan lines (that is, within 4 ms for the ‘hex’ string in Fig. 2a), usually appear rather straight, despite large lateral displacements between successive images. These observations suggest discrete ‘hex’ string jumps in which the entire string is shifted within a few milliseconds, separated by larger periods of inactivity. As visible in Fig. 3a, facile lateral motion is only observed in isolated ‘hex’ strings and not in wider domains, consisting of two or more ‘hex’ strings. Attachment of a ‘hex’ string to another isolated string or to a wider domain immediately results in its immobilization.

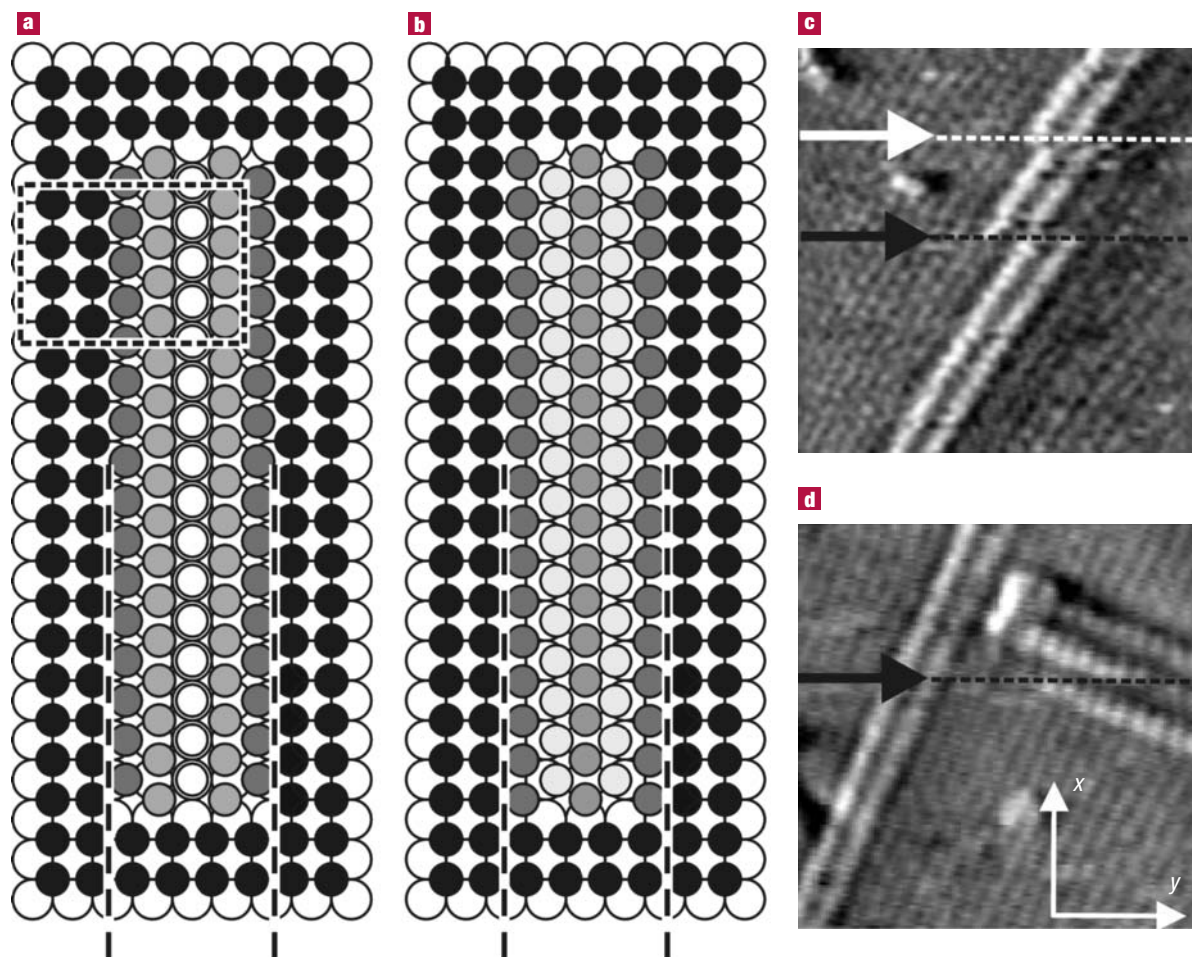


Figure 1 Atomic-scale structure and mobility of isolated 'hex' strings in the Au(100)-(1×1) surface. **a, b**, Models of the two types of strings. The small black and shaded circles denote Au surface atoms in fourfold-hollow sites, that is, the (1×1) phase, and in the 'hex' string, respectively. Large open circles indicate atoms in the underlying square lattice. The rectangular area is discussed in Fig. 3c. **c, d**, Atomic-resolution *in situ* video-STM images, taken from videos recorded at 15 frames per second **c**, $70 \times 70 \text{ \AA}^2$, **d**, $80 \times 80 \text{ \AA}^2$. Sudden lateral string displacements are indicated by arrows.

On the other hand, the mobility is independent of the string length, indicating that the highly dynamic behaviour is primarily a consequence of the nanoscale widths of the strings.

The facile lateral shift of 'hex' strings by one or two lattice constants in the perpendicular direction can be explained by small displacements of the atoms within and along the hexagonally ordered strip of Au surface atoms (see Fig. 1a,b). As a high mobility was even observed for strings of several hundred ångströms in length (consisting of more than 1,000 Au surface atoms), a truly collective motion is improbable. More likely, the displacements occur through propagation of structurally relaxed kinks along the string, that is, through mobile structural distortions that extend over a distance Δx_{kink} and involve local string bending (see the model in Fig. 2c). This is supported by observations of 'hex' domains consisting of two strings, where the propagation of such relaxed kinks can be directly followed in the video sequences (Fig. 2b). As double and single 'hex' strings are, apart from their larger width, structurally identical, the mechanisms of surface dynamics should also be identical. In double strings, however, twice the number of atoms has to be shifted in each elementary step of the kinks motion (that is, during the displacement of the kink along the string by one lattice spacing d_{Au}), resulting in a much slower kink propagation rate of only $\approx 100 \text{ \AA s}^{-1}$.

Assuming that the effective activation barrier E_d for kink motion in double strings is twice that in single strings, and using conventional attempt frequencies (10^{11} s^{-1} ; ref. 16), a value $E_d \approx 0.5 \text{ eV}$ and a propagation rate for kinks in single strings of the order of $v_{\text{kink}} = 100 \text{ \mu m s}^{-1}$ can be estimated. The time scales obtained by this crude model seem plausible considering recent observations of rapid dislocation glide motion at metal surfaces¹⁷, and are in accordance with our STM observations on single-string dynamics. Kinks corresponding to string jumps by one lattice spacing d_{Au} and a second type of kink corresponding to jumps of $2d_{\text{Au}}$ may also exist. In both cases each atom within the string has to be displaced by $\approx 1/2 d_{\text{Au}}$ (albeit in different directions for both types of jumps). The coexistence of two different shift mechanisms with similar jump rates is supported by a statistical analysis of this perpendicular lateral motion, currently in progress.

Even more surprising than the perpendicular displacements of 'hex' strings is the observation of rapid string motion along the string direction, as illustrated by a string 145 Å long in Fig. 3a (ends marked by arrows). Obviously, the length of the string is almost constant despite a movement by 5 to 95 Å between successive images (the neighbouring immobile strings are pinned by 'hex' domains or surface defects). This is even more evident in plots of the y positions of upper and lower string

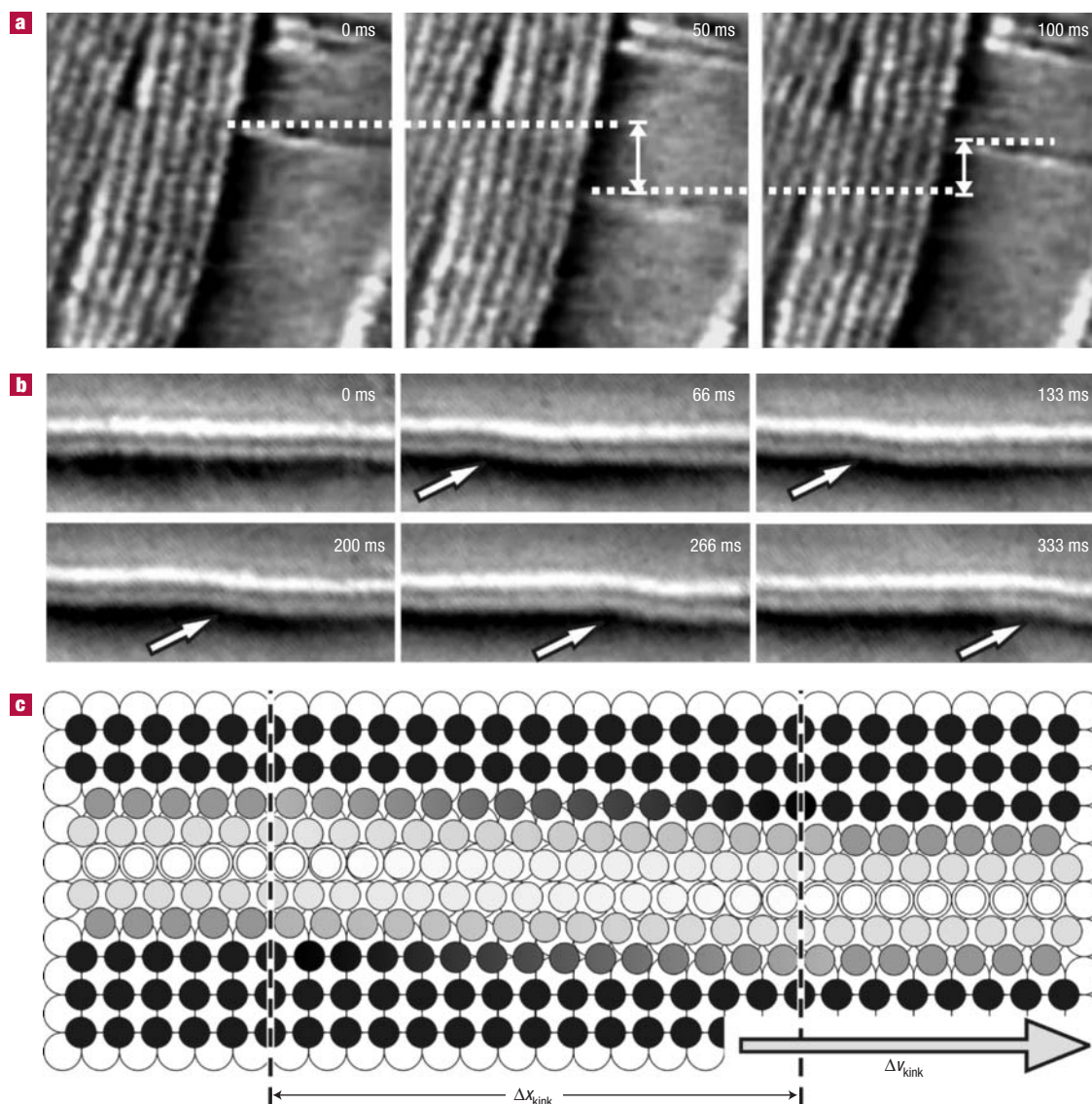


Figure 2 Motion of 'hex' strings perpendicular to the string direction. **a, b**, video-STM sequences, showing **a**, positional fluctuations of an isolated string in the x direction ($230 \times 230 \text{ \AA}^2$, 20 frames per second), and **b**, kink propagation along a double string ($120 \times 300 \text{ \AA}^2$, 15 frames per second). **c**, Model of a structurally relaxed kink in an isolated 'hex' string (extension of the kink, Δx_{kink} , indicated by dashed lines).

end versus time, as shown in Fig. 3b for a similar event. Clearly, the positional changes at the two ends of the 'hex' string are strongly correlated. Furthermore, both ends move at orders of magnitude higher rates than the ends of neighbouring (immobile) 'hex' strings, that is, much faster than the local growth of the reconstruction. This type of motion can therefore not be explained by independent growth and dissolution processes at both ends of the 'hex' string as found for example, for the motion of surface dislocations¹⁸, but requires a novel, quasi-collective mechanism.

Contrary to the displacements in the perpendicular direction, motion along the string direction requires long-range mass transfer, that is, the transport of Au atoms from the 'back' end of the string, where the 'hex' phase is transformed into the lower density (1×1) lattice (Fig. 3a, white arrows), to the 'front' end, where the hexagonally close-packed 'hex' surface layer is formed (black arrows). One important contribution to this mass transport is the propagation

of kinks as in Fig. 2c, which can be viewed as domain walls in the 'hex' adlayer and consequently exhibit a locally enhanced (heavy domain walls) or reduced (light domain walls) Au surface density (3 additional or missing Au atoms per kink corresponding to jumps by a_{Au}). A second possible mass transport mechanism is the quasi-one-dimensional diffusion of adatoms that are confined to the surface region on top of the 'hex' string. As shown in previous studies, Au adatom diffusion on reconstructed Au(100) is strongly anisotropic with the effective diffusion barriers parallel to the string direction being considerably lower than that of adatoms on the (1×1) lattice^{19–21}. However, these studies were restricted to homogeneous reconstructed or unreconstructed surfaces, and consequently cannot explain why the adatoms are confined to the 'hex' string rather than adsorbing in the energetically preferred fourfold hollow sites of the neighbouring (1×1) lattice. We therefore performed density functional theory calculations, where the specific nanoscale geometry of isolated strings,

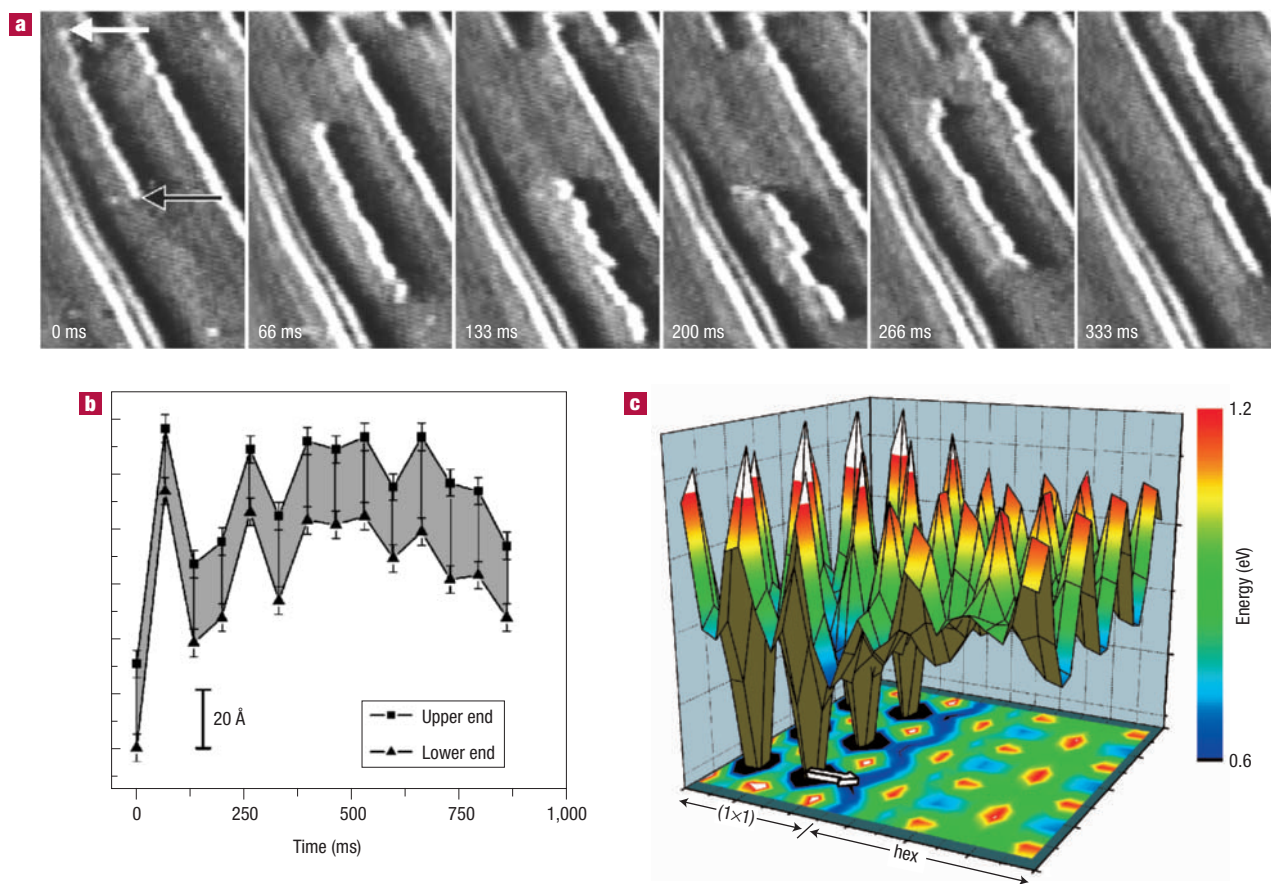


Figure 3 Motion of 'hex' strings parallel to the string direction. **a**, video-STM sequence ($180 \times 290 \text{ \AA}^2$, 15 frames per second). **b**, Position in the y direction of the upper and lower end of a mobile string as a function of time, obtained from evaluation of a video-STM sequence. **c**, Energy surface for a Au adatom on and in the vicinity of an isolated 'hex' string, obtained from density functional theory calculations (the corresponding surface area is indicated by the rectangle in Fig. 1a).

that is, the presence of 'hex'-(1×1) boundaries, was explicitly taken into account. As illustrated by the resulting energy surface for the Au adatom (Fig. 3c), the diffusion barrier on the 'hex' surface indeed is strongly reduced along the string direction as compared with diffusion on the (1×1) lattice ($\Delta E_{\text{hex}} = 0.11 \text{ eV}$ versus $\Delta E_{1 \times 1} = 0.79 \text{ eV}$ for hopping and 0.80 eV for exchange diffusion) and adsorption on the (1×1) lattice is strongly favourable (energy of adsorption in the fourfold-hollow sites is $\geq 0.56 \text{ eV}$ higher than that in the threefold-hollow sites on the 'hex' string). Furthermore, diffusion by direct hopping between neighbouring fourfold sites along the 'hex'-(1×1) boundary also has a barrier of 0.78 eV , that is, it is not preferred. However, the energy barrier for an adatom that hops onto the string from a neighbouring fourfold-hollow site (indicated by white arrow in Fig. 3c) is only $\Delta E_{1 \times 1 \rightarrow \text{hex}} = 0.66 \text{ eV}$, that is, 0.13 eV lower than $\Delta E_{1 \times 1}$. Consequently, a string-assisted hopping process with a lower effective barrier than $\Delta E_{1 \times 1}$ exists, where an adatom hops from a fourfold site onto the string, moves one or several lattice constants on the string, and then falls back into a neighbouring fourfold site. This opens up a new pathway of rapid one-dimensional diffusion along the 'hex' string boundaries. As can be seen in other video-STM sequences (not shown), both microscopic mass transport mechanisms are also effective in the growth of the 'hex' strings and therefore directly affect the kinetics of the 'hex' \rightarrow (1×1) transition.

Our video-STM observations of nanoscale 'hex' strings in the Au(100) surface demonstrate that even an apparently simple material such as an elemental metal may exhibit a surprisingly complex dynamic behaviour. In fact, the quasi-collective lateral types of motion discussed here are only the most simple processes involving 'hex' strings. For example, attractive interactions between neighbouring 'hex' strings resulting in the formation of larger 'hex' domains, the breaking of strings into two, independently moving parts, the recombination of two strings, and transient disordering of large sections of strings have been observed. Similar dynamic phenomena can be expected during phase transitions and growth processes in structurally similar systems^{6,7}. Due to their simple, well-defined structure, the rich dynamic phenomena, as well as the good agreement between the rates of these processes and the time-resolution accessible by STM, isolated 'hex' strings provide an interesting model system for future detailed studies of the dynamic behaviour of nanoscale objects.

METHODS

STM video sequences 1–3 min long were recorded at image acquisition rates of 10 to 20 images per second in 'constant height' mode (using Apiezon-coated W tips, average tunnelling currents of 1–3.5 nA, and 50 mV tunnelling bias) with the slow scan direction running from bottom to top. Images are low-pass filtered to appear as if illuminated from the left. The Au(100) sample was prepared by flame annealing, transferred in the electrochemical cell of the STM, and then covered under potential control

by 0.01 M Na₂SO₄ + 0.001 M HCl, prepared from suprapure Na₂SO₄ and HCl (Merck) and from ultrapure water. Adsorbed Cl⁻ enhances the Au surface mobility and was added to remove Au islands from the initial unreconstructed surface at 0.45 V. At the potential of the dynamic studies (-0.1 V) Cl⁻ is almost completely desorbed and should only have a small effect on the surface dynamics. The density functional theory calculations were performed with the local-density approximation for the exchange-correlation functional, as implemented in the FHI98md code. A (7×2) surface unit cell with the long side crossing the entire 'hex' string; a slab thickness of 5 layers (allowing the top layer and the adatom to relax) and 6 Å of vacuum; a plane-wave basis set with a cut-off energy of 30 Ry; and 4 k points in the surface Brillouin zone were used.

Received 11 February 2003; accepted 24 September 2003; published 2 November 2003.

References

1. Brune, H. Microscopic view of epitaxial metal growth: nucleation and aggregation. *Surf. Sci. Rep.* **31**, 121–229 (1998).
2. Giesen, M. Step and island dynamics at solid vacuum and solid/liquid interfaces. *Prog. Surf. Sci.* **68**, 1–153 (2001).
3. van Hove, M. A. *et al.* The surface reconstructions of the (100) crystal faces of iridium, platinum and gold. *Surf. Sci.* **103**, 189–217 (1981).
4. Rieder, K. H., Engel, T., Swendsen, R. H. & Manninen, M. A helium diffraction study of the reconstructed Au(100) surface. *Surf. Sci.* **127**, 223–242 (1983).
5. Gibbs, D., Ocko, B. M., Zehner, D. M. & Mochrie, S. G. J. Structure and phases of the Au(001) surface-inplane structure. *Phys. Rev. B* **42**, 7330–7344 (1990).
6. Naumovets, A. G. in *Phase Transitions and Adsorbate Restructuring at Metal Surfaces* vol. 7. (eds King, D. A. & Woodruff, D. P.) 163–213 (Elsevier, Amsterdam, 1994).
7. Magnussen, O. M. Ordered anion adlayers on metal electrode surfaces. *Chem. Rev.* **102**, 679–725 (2002).
8. Kolb, D. M. Reconstruction phenomena at metal-electrolyte interfaces. *Prog. Surf. Sci.* **51**, 109–173 (1996).
9. Kolb, D. M. & Schneider, J. The study of reconstructed electrode surfaces: Au(100)-(5×2). *Surf. Sci.* **162**, 764–775 (1985).
10. Ocko, B. M., Wang, J., Davenport, A. J. & Isaacs, H. S. In situ X-ray reflectivity and diffraction studies of the Au(001) reconstruction in an electrochemical cell. *Phys. Rev. Lett.* **65**, 1466–1469 (1990).
11. Gao, X., Hamelin, A. & Weaver, M. J. Potential-dependent reconstruction at ordered Au(100)-aqueous interfaces as probed by atomic-resolution scanning tunneling microscopy. *Phys. Rev. Lett.* **67**, 618–621 (1991).
12. Gao, X. & Weaver, M. J. Electrode potential-induced reconstruction of Au(100): Effect of chemisorption on nanoscale dynamics as probed by in-situ scanning tunneling microscopy. *J. Phys. Chem.* **97**, 8685–8689 (1993).
13. Magnussen, O. M., Hotlos, J., Behm, R. J., Batina, N. & Kolb, D. M. An in-situ scanning tunneling microscopy study of electrochemically induced 'hex' <-> transitions on Au(100) electrodes. *Surf. Sci.* **296**, 310–332 (1993).
14. Zitzler, L., Gleich, B., Magnussen, O. M. & Behm, R. J. Electrochemical video-STM. *Proc. Electrochem. Soc.* **99–28**, 29–38 (2000).
15. Magnussen, O. M., Zitzler, L., Gleich, B., Vogt, M. R. & Behm, R. J. In-situ atomic-scale studies of the mechanisms and dynamics of metal dissolution by high-speed STM. *Electrochim. Acta* **46**, 3725–3733 (2001).
16. Nabarro, F. R. N. *Dislocations in solids* vol. 3. (North-Holland, Amsterdam, 1983).
17. de la Figuera, J. *et al.* Direct observation of misfit dislocation glide on surfaces. *Phys. Rev. Lett.* **86**, 3819–3822 (2001).
18. Schmid, A. K., Bartelt, N. C., Hamilton, J. C., Carter, C. B. & Hwang, R. Q. Brownian motion of dislocations in thin films. *Phys. Rev. Lett.* **78**, 3507–3510 (1997).
19. Günther, S., Kopatzki, E., Bartelt, M. C., Evans, J. W. & Behm, R. J. Anisotropy in nucleation and growth of two-dimensional islands during homoepitaxy on 'hex' reconstructed Au(100). *Phys. Rev. Lett.* **73**, 553–556 (1994).
20. Bönig, L., Liu, S. & Metiu, H. An effective medium theory study of Au islands on the Au(100) surface: reconstruction, adatom diffusion, and island formation. *Surf. Sci.* **365**, 87–95 (1996).
21. Yu, B. D. & Scheffler, M. Physical origin of exchange diffusion on f.c.c.(100) metal surfaces. *Phys. Rev. B* **56**, R15569–R15572 (1997).

Acknowledgements

We gratefully acknowledge financial support by the Deutsche Forschungsgemeinschaft and a fellowship for M.L. by the Alexander von Humboldt-Stiftung. Correspondence and request for materials should be addressed to O.M.M. Supplementary Information accompanies the paper on www.nature.com/naturematerials

Competing financial interests

The authors declare that they have no competing financial interests.